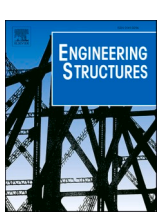
ELSEVIER

Contents lists available at ScienceDirect

Engineering Structures

journal homepage: www.elsevier.com/locate/engstruct



Influence of corrosion on nonlinear tension stiffening of concrete under monotonic and cyclic loading

Ehsan Ahmadi ^{a,*}, Hammed Aminulai ^b, Mohammad M. Kashani ^b

ARTICLE INFO

Keywords: Tension stiffening of concrete Corroded RC specimens Monotonic and cyclic tests DIC

ABSTRACT

Reinforced concrete (RC) structures are highly susceptible to reinforcement corrosion, which leads to a significant reduction in their structural capacity. Corrosion particularly affects the bond between concrete and steel reinforcement in RC members, affecting the tensile capacity of the uncracked concrete between cracks—a phenomenon known as tension stiffening. Existing research on tension stiffening behaviour in corroded RC members has primarily focused on low corrosion levels under monotonic loading, leaving gaps in understanding its behaviour at higher corrosion levels or under cyclic loading. This study addresses these gaps by experimentally investigating the effects of corrosion on the nonlinear tension stiffening behaviour of RC members under both monotonic and cyclic loading, across a range of corrosion levels. A total of 28 RC specimens, including uncorroded and artificially corroded specimens, were tested under uniaxial tension. Crack formation and propagation were monitored using Digital Image Correlation (DIC). The results demonstrate that corrosion significantly reduces the tension stiffening of concrete, with larger steel bar sizes exacerbating this effect. Furthermore, current models are insufficient in prediction of crack spacing and width of corroded structural elements, which highlight the need for more robust and reliable models.

1. Introduction

In recent years, infrastructure deterioration has emerged as a critical global challenge. Among reinforced concrete (RC) structures, the corrosion of steel reinforcement has proven to be a major factor contributing to the degradation of functionality and longevity [1-3]. Corrosion in RC structures typically initiates via two primary mechanisms: (1) when the carbonation front in the concrete cover reaches the reinforcing steel bars without significant chloride content [4], and (2) when the chloride concentration in the pore water adjacent to the reinforcing steel bars exceeds a critical threshold [4]. Once initiated, corrosion significantly compromises the integrity of the concrete cover and diminishes the mechanical properties of the steel reinforcement [5-8]. Specifically, it results in concrete cover cracking [9-13], a reduction in steel strength [14], and a decrease in the cross-sectional area of steel bars [15]. Collectively, these effects deteriorate the structural performance of RC members, threatening their operational safety and long-term durability [16,17].

To ensure the continued safety and functionality of RC structures, thorough performance assessment is essential. Traditionally, the tensile

Tension stiffening shows the ability of concrete to sustain load between cracks within the elastic region. This effect helps in the assessment of the post-cracking behaviour of concrete. Hence, it is the difference between the response of the reinforcing bar and the RC element under tensile loading (Bischoff 2001, 2003) and results from the bond between the concrete and steel reinforcement [21,22]. Most investigations into tension stiffening have been on plain RC [23] or fibre (steel, glass or carbon) reinforced concrete [21,24,25], with very little on corroded concrete RC elements. Also, many of these works are uses analytical and numerical modelling to investigate the tension stiffening responses of such elements to loading [26–28]. Hence, there is a need to investigate the effect of corrosion on the tension stiffening of corroded RC elements.

E-mail address: Ehsan.Ahmadi@Farrat.com (E. Ahmadi).

^a Farrat Isolevel, Altrincham, Manchester, UK

^b University of Southampton, Southampton, UK

strength of cracked concrete is often disregarded in structural evaluations. However, even after cracking, the intact concrete between adjacent cracks continues to contribute to the tensile strength of RC members due to the bond between the concrete and the embedded steel reinforcement. This phenomenon, known as tension stiffening, enhances the stiffness of RC members beyond that of bare reinforcing steel [18–20], as illustrated in Fig. 1.

^{*} Corresponding author.

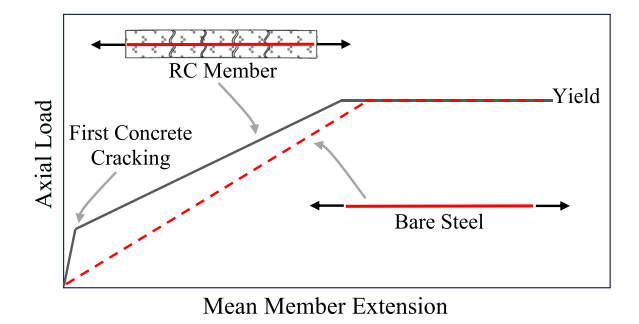


Fig. 1. Uniaxial tensile behaviour of RC members and tension stiffening effect.

Corrosion has a pronounced impact on the concrete-steel bond [29–34], thereby altering the tension stiffening behaviour of concrete. In the initial stages of corrosion, bond strength may increase due to the expansive pressure exerted by corrosion products. However, as corrosion progresses beyond a critical threshold (e.g., 0.3 %-4 % [35]), bond strength deteriorates significantly. Once the concrete cover cracks, bond capacity drops sharply, leading to a substantial reduction in tension stiffening [33,34].

Extensive research has explored the effects of corrosion on the load-bearing capacity of RC beams and columns [36]. For instance, detailed investigations into the flexural and shear performance of corroded RC beams can be found in the literature [36–41]. Similarly, the axial and flexural performance of corroded RC columns has been thoroughly studied [17,42–50]. However, there is a notable lack of comprehensive research on the tension stiffening behaviour of corroded RC members.

Most existing studies have focused on the local interfacial bond behaviour between steel and concrete under monotonic loading conditions, typically using pull-out tests [29,32–34]. These tests, conducted on small-scale specimens, tend to produce localized bond-slip behaviour that does not fully represent the global tensile performance of full-scale RC members. A rare study on the tensile behaviour of full-scale corroded RC members examined only three specimens, two of which were artificially corroded up to 4 %, under monotonic loading conditions [51]. This limited scope underscores the need for further investigation into the effects of higher corrosion levels and cyclic loading on tension stiffening.

In summary, while there is extensive knowledge regarding the compressive, shear, and flexural performance of corroded RC members, their tension stiffening behaviour remains inadequately studied. This study presents several novel contributions to the understanding of corrosion-induced degradation in reinforced concrete members under tension. This paper is the second experimental investigation (after the work in [51]) focused on the tension-stiffening behaviour of corroded RC members. The experimental programme is comprehensive, involving 28 specimens tested under both monotonic and cyclic loading across a range of corrosion levels, from uncorroded to highly corroded conditions. Moreover, the influence of the concrete cover-to-bar diameter ratio on cracking characteristics and stiffness degradation is systematically explored, offering new insights into parameters that have received limited attention in prior studies. These aspects collectively enhance the practical relevance and originality of the current study.

This study seeks to address this gap by investigating the impact of corrosion on tension stiffening in RC members. The research focuses on theoretical corrosion levels up to 20 % under both monotonic and cyclic loading conditions. A detailed experimental programme was undertaken, involving the mechanical characterization of steel and concrete materials, the preparation of artificially corroded RC specimens, and uniaxial tensile testing. The tension stiffening behaviour of the specimens was characterized using uniaxial tensile tests and monitored through Digital Image Correlation (DIC) techniques.

2. Experimental programme

To evaluate the impact of reinforcement corrosion on the tension stiffening behaviour of full-scale concrete members, 28 reinforced concrete (RC) specimens were fabricated and tested under uniaxial tension. These tests were conducted at the Testing and Structures Research Laboratory (TSRL) at the University of Southampton. Among the specimens, 14 were tested under monotonic loading, and 14 under cyclic loading. Table 1 provides an overview of the RC specimens tested for each loading type and target corrosion levels.

For each combination of loading type and reinforcement size (Φ 20 or Φ 25), 3 specimens were left uncorroded, serving as benchmarks (0 % corrosion). The remaining 4 specimens were artificially corroded to target levels of 5 %, 10 %, 15 %, and 20 % using an accelerated corrosion procedure (see 2.2).

2.1. RC specimens and material characterisation

The RC specimens used for uniaxial tensile testing are shown schematically in Fig. 2. Each specimen measures 1050 mm in length with a square cross-section of 100×100 mm. The steel reinforcement, positioned at the centre, consisted of B500B ribbed steel bars conforming to BS EN 10080:2005 [52] and BS 4449:2005 + A3:2016 [53] standards. The concrete encases 800 mm of the steel bar, while 125 mm at each end remains exposed for testing. Two steel bar diameters (Φ 20 mm and Φ 25 mm) were selected to assess the effect of bar size on tension stiffening behaviour.

The construction process for the RC specimens is shown in Fig. 3. Timber moulds were prepared, and steel bars were placed centrally within the moulds (Fig. 3a). Concrete was poured and compacted (Fig. 3b), followed by curing for 28 days after mould removal (Fig. 3c). Black grease was applied to the exposed ends of each specimen to prevent corrosion during testing (Fig. 3c).

Before fabricating the RC specimens, the mechanical properties of the concrete and steel reinforcement were determined. Two tests were performed on concrete: (1) Compression Test: Six $100 \times 100 \times 100$ mm cubes were tested, yielding a mean compressive strength of 40 MPa, and (2) Four-Point Flexural Test: Two $100 \times 100 \times 500$ mm beams were tested according to BS EN 12390–5:2019 [54], resulting in a mean tensile strength of 2.85 MPa (Figs. 4 and 5). The concrete was tested for compressive and flexural strengths at 60 days.

Steel reinforcement bars were subjected to tensile tests using a 630 kN servo-hydraulic Schenck machine. Tests adhered to BS EN 10080:2005 [52] and BS 4449:2005 + A3:2016 [53], with strain rates applied as per BS EN ISO 6892–1:2019 [55]. A 50 mm dynamic extensometer recorded extensions during loading. The stress-strain curves for $\Phi 20$ and $\Phi 25$ bars are shown in Fig. 6, and the mechanical properties are summarized in Table 2.

2.2. Accelerated corrosion procedure

Natural corrosion of reinforcement is a lengthy process, unsuitable for laboratory experiments [56]. Instead, an accelerated electrochemical procedure was employed, which has been shown to produce similar outcomes to natural corrosion [57]. In this work, artificial corrosion was used in a controlled laboratory space through an accelerated electrochemical process, which exhibited similar results to the natural

Table 1Number of RC specimens tested for each loading type.

Steel Bar Size	Target Corrosion Levels						
	0 %	0 % 5 %		15 %	20 %		
Ф20	3	1	1	1	1		
Φ25	3	1	1	1	1		

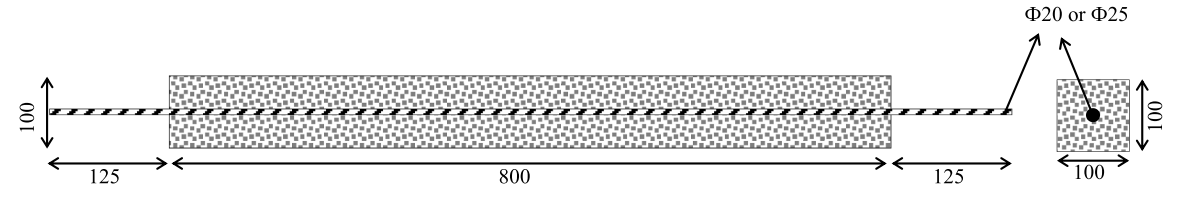
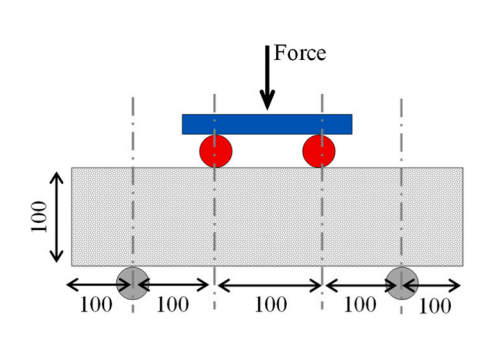


Fig. 2. RC specimens for uniaxial tensile testing (dimensions in mm).



Fig. 3. Manufacturing process of the RC specimens: (a) timber moulding and reinforcement placement, (b) concrete casting and compaction, and (c) mould removal and end greasing.



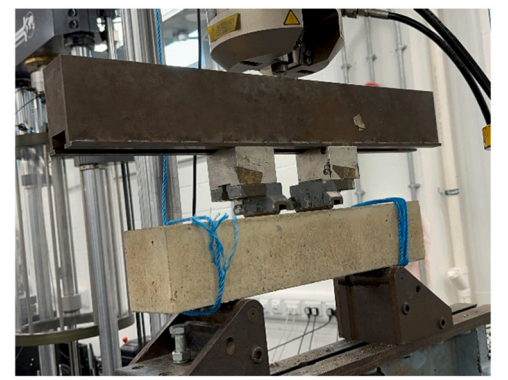


Fig. 4. Four-point flexural test setup (dimensions in mm).

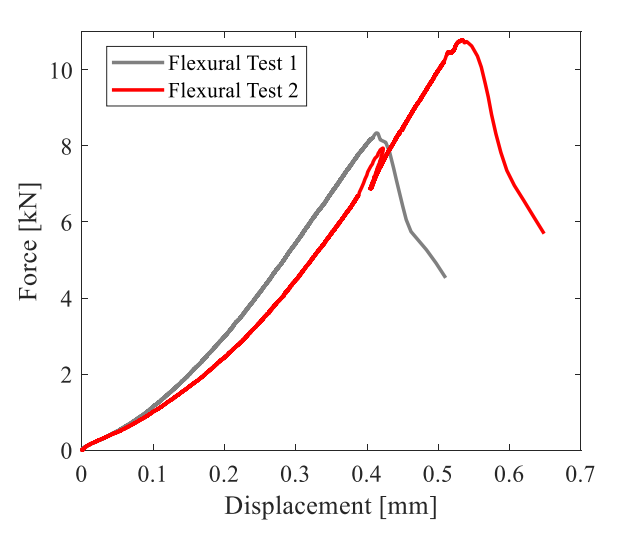


Fig. 5. Concrete flexural tests, force-displacement curves.

corrosion [56,58,59]. Fig. 7 schematically shows the accelerated corrosion of the RC specimens conducted in the current study. Each RC specimen, selected to be corroded, are initially immersed in 10 % sodium chloride (NaCl) solution. Afterwards, a DC power supply is passed through the solution. The cathode (i.e., negative node) is connected to the steel bar and the anode (i.e., positive node) is connected to the stainless steel placed around the immersed specimen. Then, the DC power supply is tuned to provide a contact current of 2 Amp. The Faraday's second law of electrolysis [8] is adopted to estimate the time duration required for the target corrosion levels in Table 1. However, the actual mass losses due to corrosion are different from the target losses. To measure the actual mass losses (i.e., actual corrosion levels) after the corrosion process, the corroded steel bars are detached from the RC specimens after tensile tests (2.3) and immersed in vinegar to remove the rust and concrete on the steel bars. Afterwards, the steel's surface is polished using a wire brush according to ASTMG1-03 [60], which removes remaining concrete and rust particles. The actual mass caused by corrosion is then given by:

$$\gamma = \frac{m_{\rm u} - m_{\rm c}}{m_{\rm u}} \times 100 \tag{1}$$

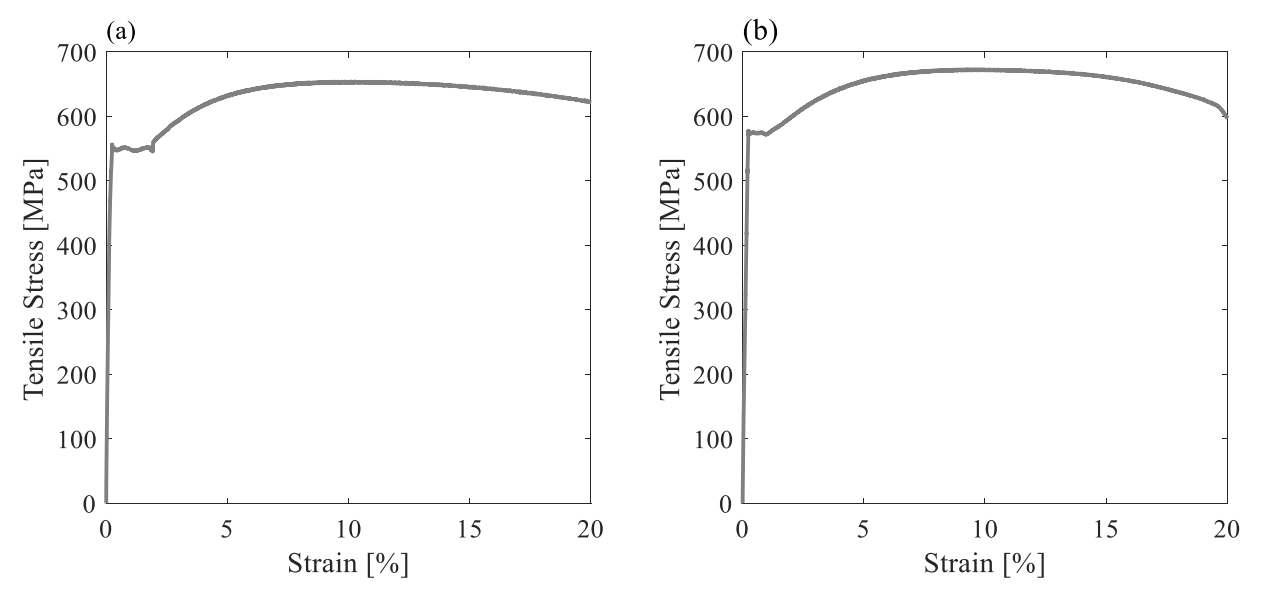


Fig. 6. Stress-stain curves of the steel bars: (a) Φ 20, and (b) Φ 25.

Table 2
Material characterisation results.

Property	Mean Value (MPa)
Concrete Compressive Strength (cube)	40
Concrete Tensile Strength	2.85
Reinforcement Yielding Strength (Φ20)	550
Reinforcement Yielding Strength (Φ25)	576
Reinforcement Ultimate Strength (Φ20)	653
Reinforcement Ultimate Strength (Φ25)	671

where m_u and m_c are the mass per unit length of the uncorroded and corroded bars, respectively; γ is the average corrosion level (i.e., average mass loss) across the length of the bar.

2.3. Instrumentation and uniaxial tensile tests

The RC specimens are tested under uniaxial monotonic tensile loading and uniaxial cyclic tensile loading. The load is exerted through the displacement control mode by the servo-hydraulic Instron Schenck 630 kN testing machine available in the TSRL (see Fig. 8).

The machine uses an internal Linear Variable Differential Transformer (LVDT) that measures the displacement of the actuator during loading. Additionally, an internal load cell measures the load resulting from the applied displacement. The test setup is shown in Fig. 8a. The axial displacement at the middle 600 mm part of the RC specimens is measured by the two LVDTs that are externally attached to each side of the specimens and are recoded via a multichannel data acquisition unit

(Strainsmart 8000). For the monotonic loading, a total displacement of 12 mm is applied to the RC specimens with displacement rate 0.024 mm/s or strain rate of 0.0003 strain/s. Thus, the entire duration of each monotonic test is 8.33 mins, and the maximum strain applied is 0.015. The cyclic loading pattern is composed of 8 cycles with 4 different mean strains, each strain peak repeating twice, as shown in Fig. 8b-d. The mean strain values are calculated using the results of the monotonic tests. All strain peaks are applied at the rate of 0.0003 strain/s that is equivalent to displacement rate of 0.024 mm/s.

2.4. Digital image correlation (DIC) of specimens

A digital image correlation (DIC) is a non-destructive, non-contact, full-field optical measurement technique capable of capturing digital images of the surface of a specimen to obtain the in-plane strains and out-of-plane deformations in its 2D and 3D configurations. The DIC was used simultaneously with the LVDTs to capture the crack propagation and deformations at the middle section of the RC specimens under tensile load for monotonic tests. The video imaging is performed using MatchID imaging software involving Imager E-Lite 5 M cameras fitted with Nikon AF Nikkor 28 mm f/2.8D (28 mm focal length and 2.8 maximum aperture) lens. The camera was calibrated to capture the RC tensile specimens' vertical displacements and crack formations during loading using the dots marked on the specimens. The images recorded were further processed using MatchID software to see the strain distribution resulting from the applied loading. The parameters used in the DIC image acquisition and processing are summarised in Table 3.



Fig. 7. The accelerated corrosion process conducted in this study.

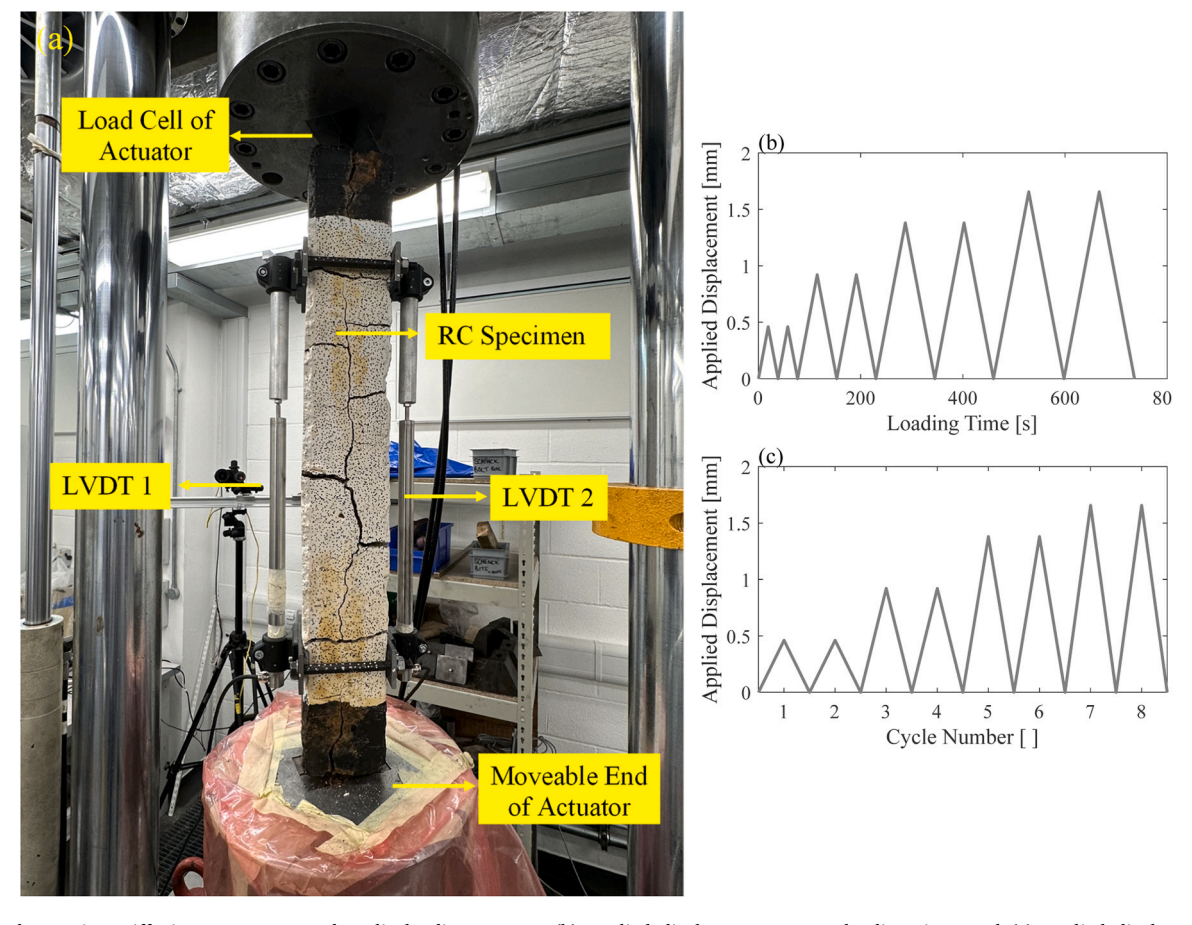


Fig. 8. (a) The tension stiffening test setup, and cyclic loading pattern: (b) applied displacement versus loading time, and (c) applied displacement versus cycle number.

Table 3 DIC processing parameters.

Technique used	2D DIC
Camera	
Camera name	Imager E-lite 5 M
Focal length	28.4621 mm
Exposure time and recording rate	19000 μs, 1 Hz
RMS of fit	0.303396 pixel
Size of dewarped image	1961×2479 pixel
Resolution	3.45μm
Processing	
Subset, step	53, 17
Matching correlation criterion	ZNSSD
Shape function	Affine
Interpolation function	Local bicubic splines
Prefiltering	Gaussian
Strain	
Smoothing method	None
Strain window	7 pixels (24.15 μm)
Virtual strain gauge	117 pixels
Mean strain resolution	524 με
Calculation mode	accurate

3. Experimental test results and discussion

The experimental tests conducted on the 28 reinforced concrete (RC) specimens provided valuable insights into the effect of reinforcement corrosion on the tension stiffening behaviour of RC members under both monotonic and cyclic loading conditions. While the target corrosion levels were defined for the specimens (5 %, 10 %, 15 %, and 20 %), the actual corrosion levels varied due to various factors in the accelerated

corrosion process. These actual corrosion levels were carefully measured after the tests using a mass loss calculation, as described in 2.2, and are summarized in Table 4. Despite the discrepancies, the measured corrosion levels were sufficiently close to the target values, confirming the effectiveness of the artificial corrosion procedure used in this study. However, due to the differences in actual corrosion levels between the monotonic and cyclic specimens, direct comparison of their results is not entirely straightforward.

Fig. 9 shows the monotonic test results for the 20 mm-diameter RC specimen alongside those of the corresponding 20 mm bare steel bar under both uncorroded and corroded (18.6 %) conditions. Fig. 9a and c display the full-range axial load–strain response, while Fig. 9b and d provide a zoomed-in view focusing on the low strain range (up to 0.002) to highlight early-stage behaviour. As shown in Fig. 9a and c, at higher strain levels, the tensile force in the RC member approaches the yield strength of the bare bar for both uncorroded and corroded conditions. This behaviour is expected, as the tension-stiffening effect diminishes at larger strains, and the load is primarily carried by the reinforcement. At lower strain levels, Fig. 9b and d indicate that initial cracking in the concrete occurs at relatively small strain values,

Table 4
Actual corrosion levels.

Loading Type	Specimen Name	Actual Corrosion Levels (%)				
		5	10	15	20	
Monotonic	SMΦ20	6.3	8.4	12.4	18.3	
	SMΦ25	2.3	9.1	12.3	21.3	
Cyclic	SCΦ20	5.1	8.2	16.9	24.7	
	SCΦ25	4.3	12.0	-	22.1	

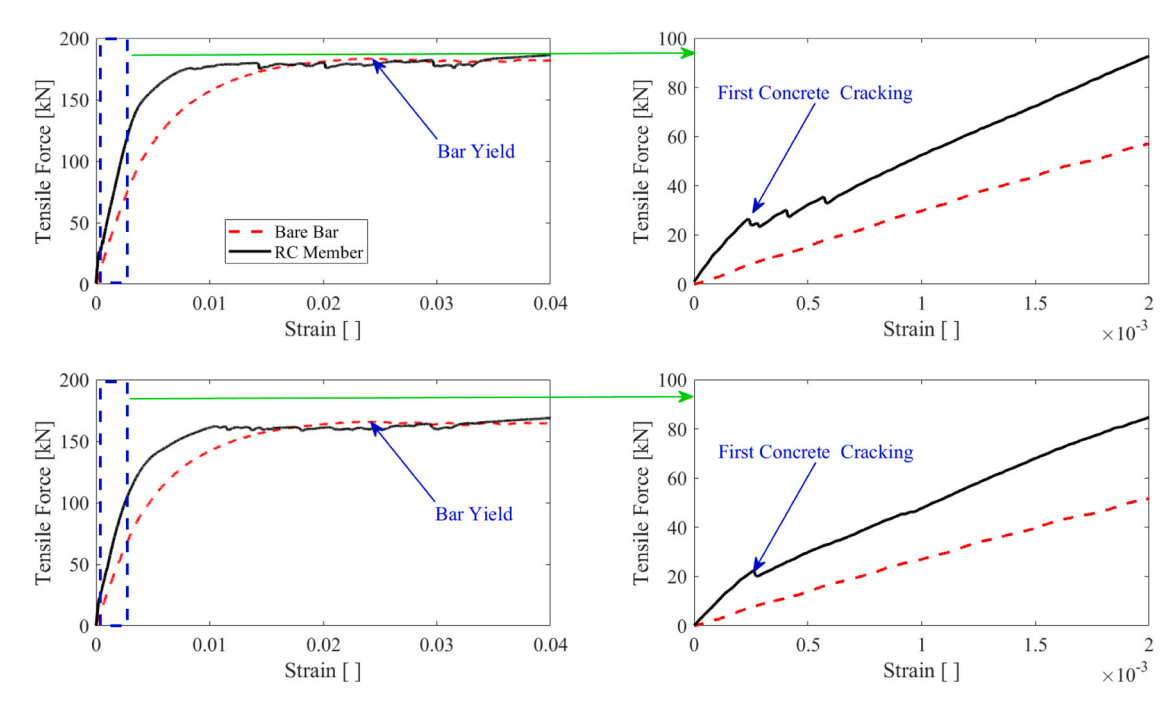


Fig. 9. Monotonic test results, SMΦ20, bare steel bar vs RC member: (a) no corrosion, (b) no corrosion, zoomed at very low strain values, (c) 18.3 % corrosion, and (d) 18.3 % corrosion, zoomed at very low strain values.

consistent with typical RC member behaviour. These comparisons support the consistency of the current experimental results with established axial tension behaviour in RC members, as shown in Fig. 1.

Fig. 10 illustrates the results for a specimen with a 20 mm diameter (40 mm concrete cover thickness) under monotonic tests. At low tensile strain rates or small extensions, the tensile capacities of both uncorroded

and corroded specimens are similar. At this stage, the concrete remains uncracked and fully bears the tensile load without significant contribution from the steel reinforcement. However, at higher tensile strain rates or larger extensions, the concrete cracks, transferring the load-bearing responsibility to the steel bar. At this point, the corrosion of the steel bar significantly reduces the tensile capacity of the specimen.

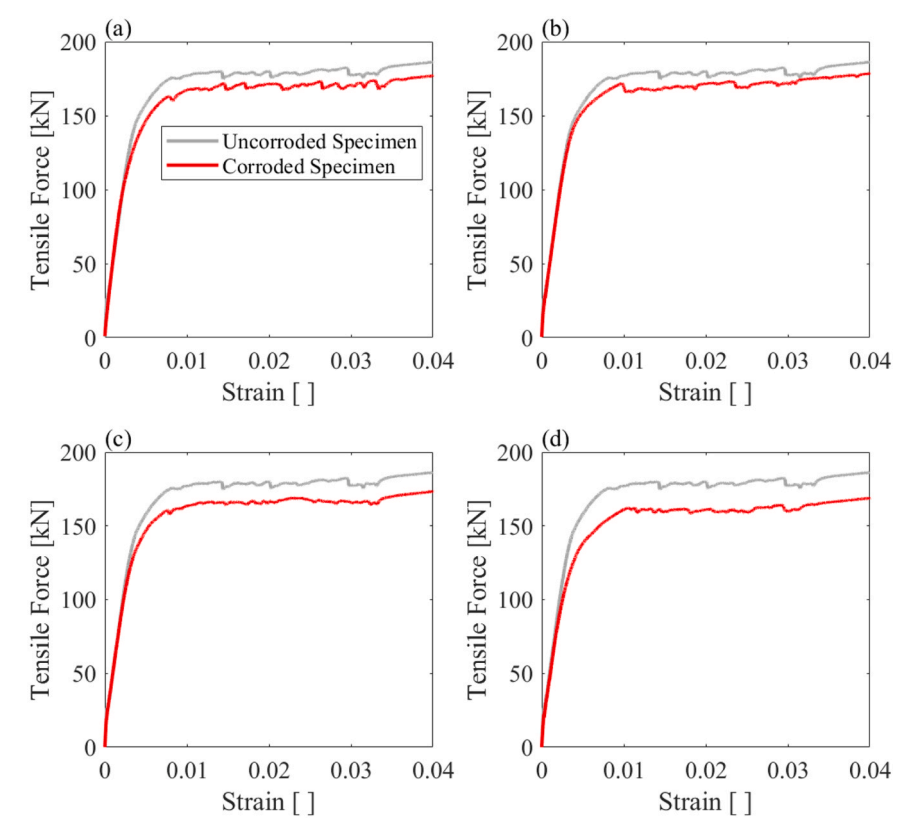


Fig. 10. Monotonic test results, SMΦ20: (a) 6.3 % corrosion, (b) 8.4 % corrosion, (c) 12.4 % corrosion, and (d) 18.3 % corrosion.

Increasing corrosion levels markedly decrease the tensile capacity and lower the tensile force or strain rate/extension threshold at which the capacities of uncorroded and corroded specimens converge.

To monitor crack formation and development, which significantly influences the tension-stiffening behaviour of concrete specimens, Fig. 11 presents the Digital Image Correlation (DIC) strain fields for specimens reinforced with 20 mm steel bars at varying corrosion levels. The DIC images depict the von Mises equivalent strain within the elastic limit of the specimens under tensile loading. For uncorroded specimens and those with lower corrosion levels (0 %, 6.3 %, and 8.4 %; Fig. 11a-c), lateral cracks were more prominent with no noticeable longitudinal crack. This indicates effective tension stiffening, as the concrete between the lateral cracks resists strain and contributes to the tensile strength of the steel bar by maintaining bond integrity. The crack opening in the uncorroded specimen is evenly distributed between three cracks. However, as the corrosion level increases, the crack pattern and opening become more uneven. For instance, (as discussed in Fig. 9b), the specimen with 8.4 % corrosion failed prematurely due to localised pitting corrosion. The DIC strain contours in Fig. 11c show that the specimen with 8.4 % corrosion has a significant crack opening in the location of crack 2, which is the location of the pitted section.

Moreover, at higher corrosion levels (12.4% and 18.3%; Fig. 11d–e), both lateral and longitudinal cracks appear. Mainly, first lateral crack was developed and at higher strain values followed by longitudinal cracks. These longitudinal cracks, induced by rebar corrosion, suggest weakened bonding or complete debonding of the steel bar from the surrounding concrete. This debonding eliminates tension

stiffening, as the concrete between the lateral cracks no longer contributes to the tensile strength of the steel bar. These results demonstrate that high corrosion levels significantly impair the tension-stiffening capacity of concrete.

Fig. 12 presents the results of cyclic tests conducted on specimens with 20 mm steel bars at various corrosion levels. At the theoretical corrosion levels of 5 % (measured corrosion = 5.1 %), the corroded specimens exhibited a slightly higher tensile force capacity compared to the uncorroded specimens. This observation aligns with findings in the literature, which indicate that at the initial stages of corrosion, bond strength tends to increase up to a threshold corrosion level (e.g., 0.3 %-4 % [27]). This phenomenon explains the observed increase in force capacity at low corrosion levels. However, at higher corrosion levels, a significant reduction in tensile force capacity is observed. Specifically, at advanced corrosion levels of 16.9 % and 24.7 %, the corroded specimens fail after only a few loading cycles. This behaviour is attributed to the combined effects of negligible tension stiffening in the surrounding concrete and the reduced capacity of the steel bars due to severe localised pitting corrosion. In addition to the diminished tensile force capacity, the highly corroded specimens exhibit significantly reduced ductility, which is a critical consideration in the design of such structural members.

To evaluate the impact of cover thickness on the tension stiffening behaviour of specimens, Fig. 13 presents the results of monotonic tensile tests conducted on specimens with a steel bar diameter of 25 mm (37.5 mm concrete cover thickness). According to Eurocode 2 [61], the minimum cover for concrete elements must be at least 2 times the bar

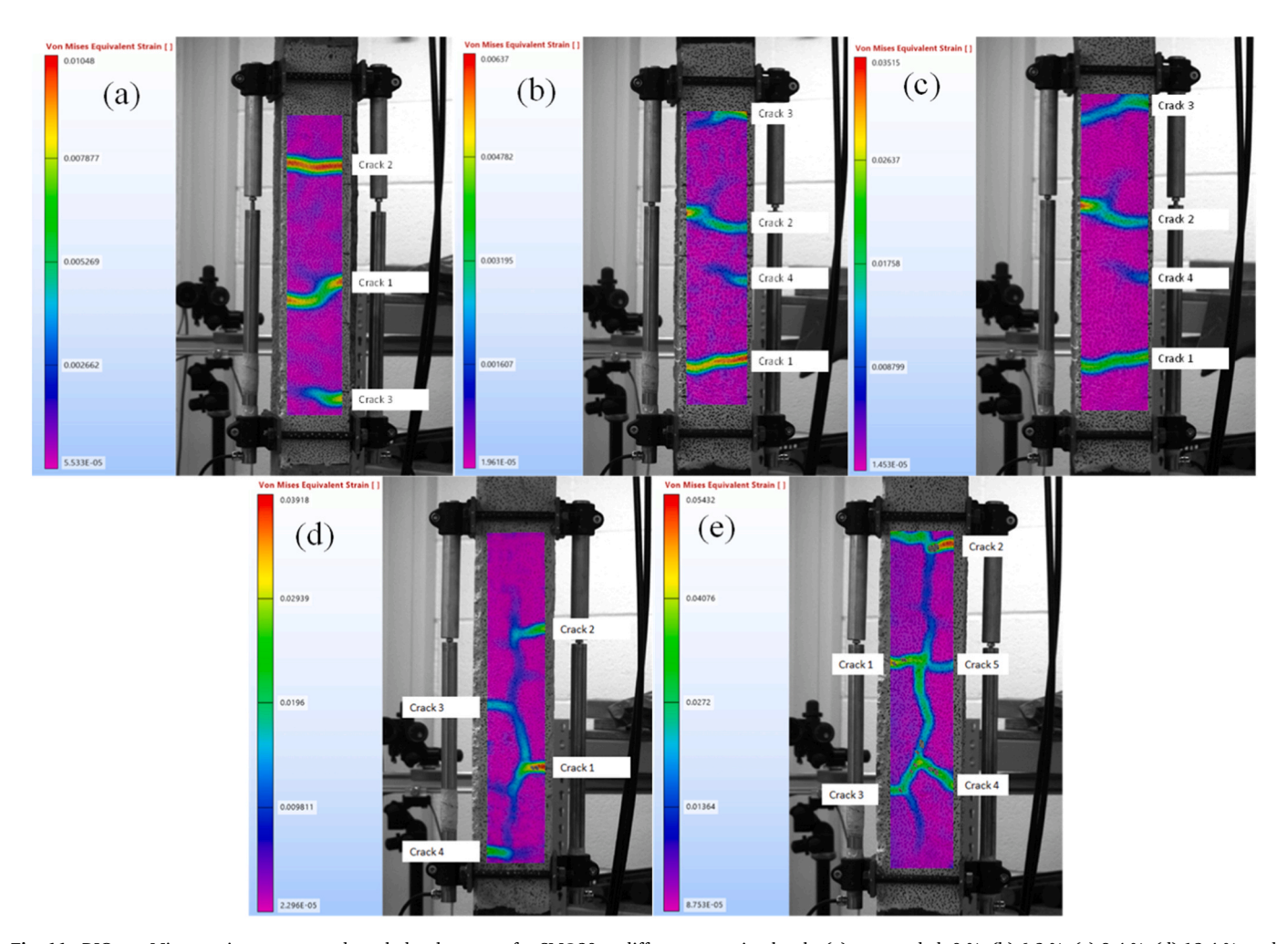


Fig. 11. DIC von Mises strain contours and crack developments for SMΦ20 at different corrosion levels: (a) uncorroded, 0 %, (b) 6.3 %, (c) 8.4 %, (d) 12.4 %, and (e) 18.3 %.

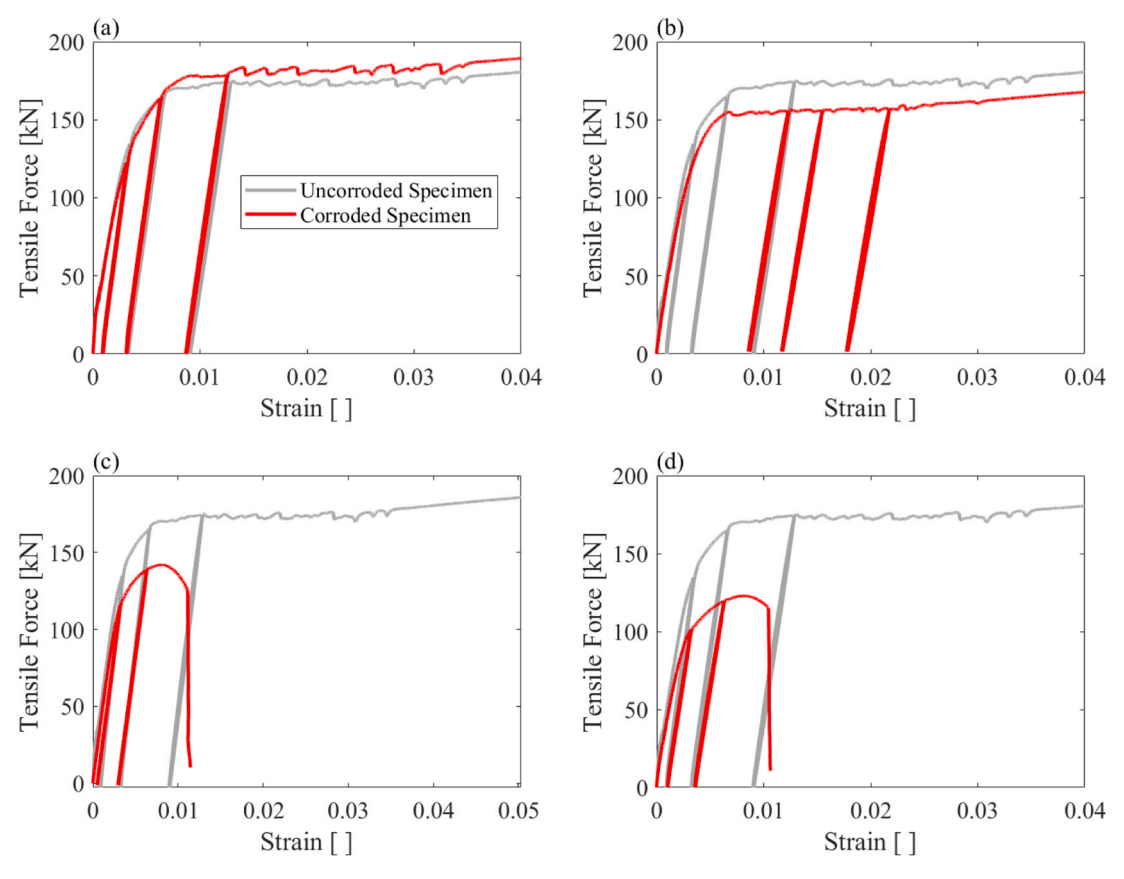


Fig. 12. Cyclic test results, SCΦ20: (a) 5.1 % corrosion, (b) 8.2 % corrosion, (c) 16.9 % corrosion, and (d) 24.7 % corrosion.

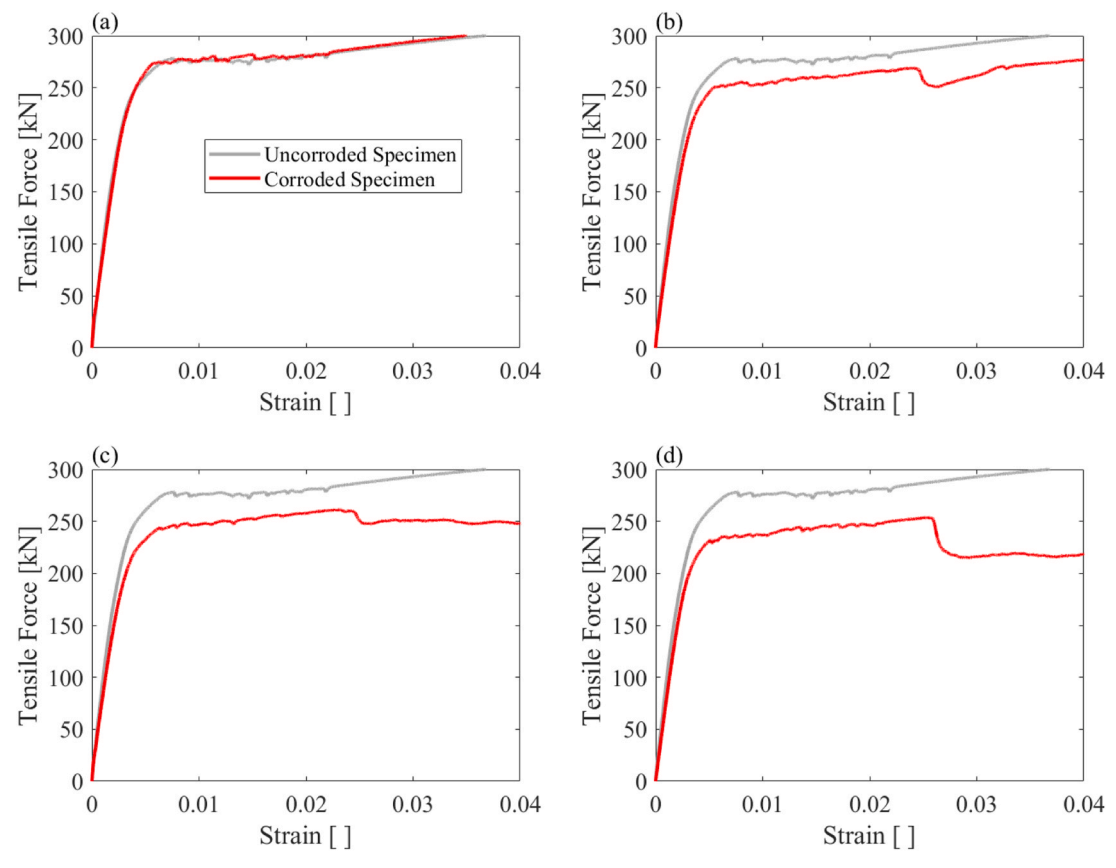


Fig. 13. Monotonic test results, SM Φ 25: (a) 2.3 % corrosion, (b) 9.1 % corrosion, (c) 12.3 % corrosion, and (d) 21.3 % corrosion.

diameter to provide full bonding between reinforcement and concrete. The specimens with 25 mm diameter bars represent old and substandard concrete structural elements that often suffer from reinforcement corrosion. As anticipated, especially at higher corrosion levels, a more pronounced reduction in the tensile force capacity of the specimens is observed. This is attributed to the fact that specimens with smaller concrete covers are more susceptible to extensive corrosion, which significantly reduces their force capacity. It is important to note that Eurocode 2 [61] provides guidelines for durability and fire protection, as well as bonding, in the design of new structures, particularly when determining the concrete cover. Additionally, at higher strain rates or extensions, a substantial decline in tensile force capacity is noted for corrosion levels of 9.1 %, 12.3 %, and 21.3 %. This behaviour is associated with the formation of longitudinal cracks in the specimens under elevated strain rates, which critically impair their tensile performance. For illustrations of these longitudinal cracks, refer to Fig. 14c-e.

Fig. 14 illustrates the Digital Image Correlation (DIC) strain fields for specimens reinforced with 25 mm diameter bars at varying corrosion levels. The images display the von Mises equivalent strain within the elastic limit under tensile loading. Similar to the behaviour observed in specimens with 20 mm steel bars, lateral cracks were initially detected in the uncorroded specimen and the specimen with a lower corrosion level of 2.3 % (Fig. 14a and b).

The DIC images indicate that at a corrosion level of about 9.1 %, longitudinal cracks began to emerge in the RC columns during loading. The longitudinal cracks started appearing during the accelerated corrosion of the specimens with higher corrosion levels (16.9 % and

24.7 % corrosion), likely due to the expansion and cracking of the concrete cover induced by the corrosion process (Fig. 14c–e). This confirms that a smaller concrete cover not only accelerates corrosion but also amplifies its impact on the debonding of the steel-concrete interface. At higher corrosion levels of 16.9 % and 24.7 %, only longitudinal cracks were observed, with lateral cracks no longer evident (Fig. 14d and e). This absence of lateral cracks indicates a marked reduction in the concrete's tension-stiffening effect, as the presence of longitudinal cracks compromises the material's ability to resist tensile forces. At the 24.7 % corrosion level (Fig. 14e), the longitudinal crack resulting from severe corrosion was significantly large. Consequently, the DIC system was unable to capture the strain field, and therefore, no DIC strain images were generated.

Compared to specimens reinforced with 20 mm diameter bars (Figs. 11 and 14), the earlier onset of longitudinal cracks at lower corrosion levels in the 25 mm diameter bar specimens highlights the accelerated reduction in the tension-stiffening capacity of concrete as bar diameter increases. This finding emphasises that inadequate concrete cover exacerbates the degradation of structural integrity under corrosive conditions.

Fig. 15 presents the cyclic test results for specimens with a steel bar diameter of 25 mm. It is important to note that the test results for a corrosion level of 15 % are unavailable due to a procedural error during testing. Unlike the cyclic test results for specimens with a steel bar diameter of 20 mm (Fig. 12), where specimens exhibited brittle failure after only a few cycles, the 25 mm steel bar specimens demonstrated a more ductile failure. These results suggest that the corrosion in these

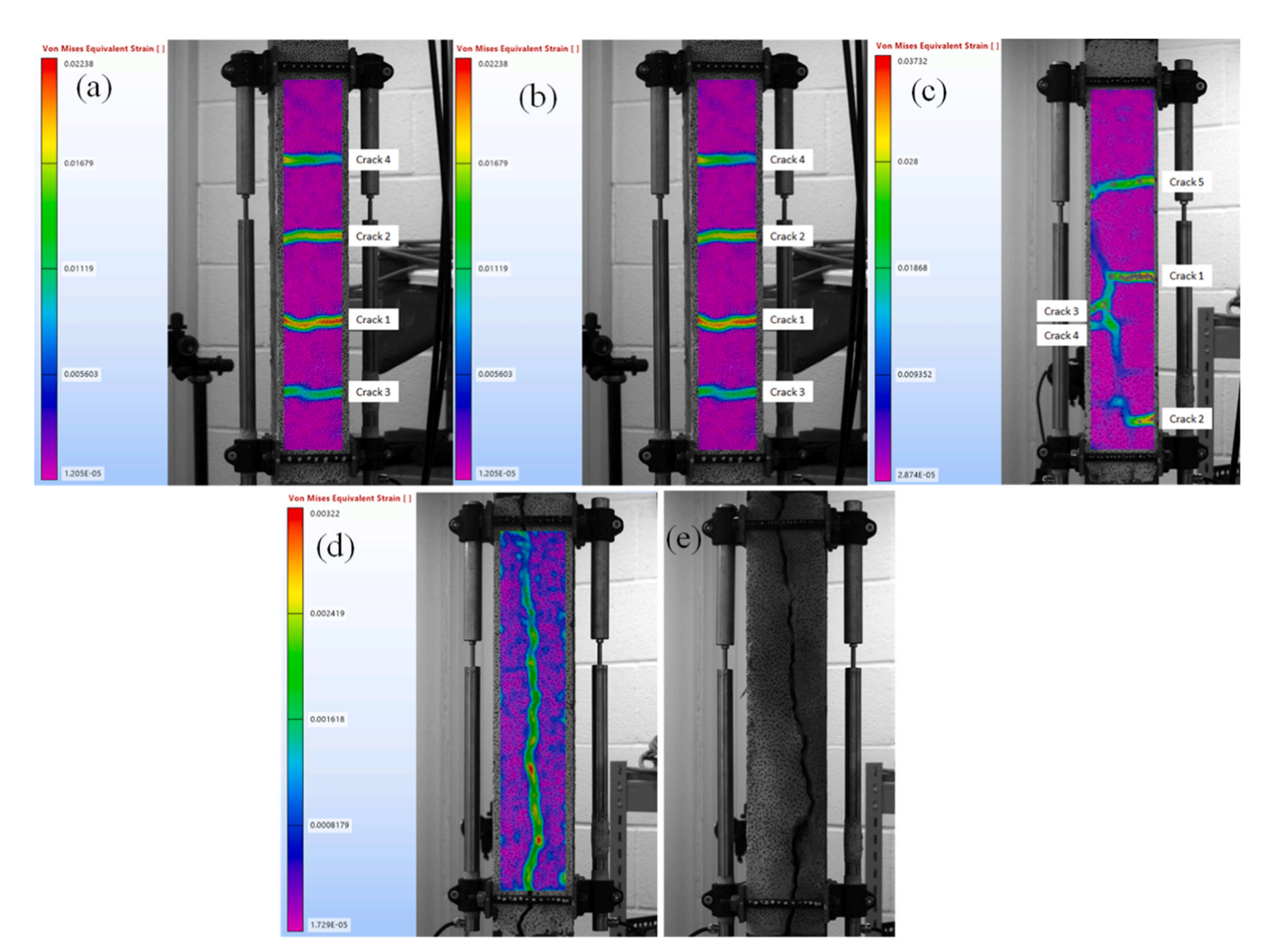


Fig. 14. DIC strain images and crack developments for SMΦ25 at different corrosion levels: (a) uncorroded, 0 %, (b) 2.3 %, (c) 9.1 %, (d) 16.9 %, and (e) 24.7 %.

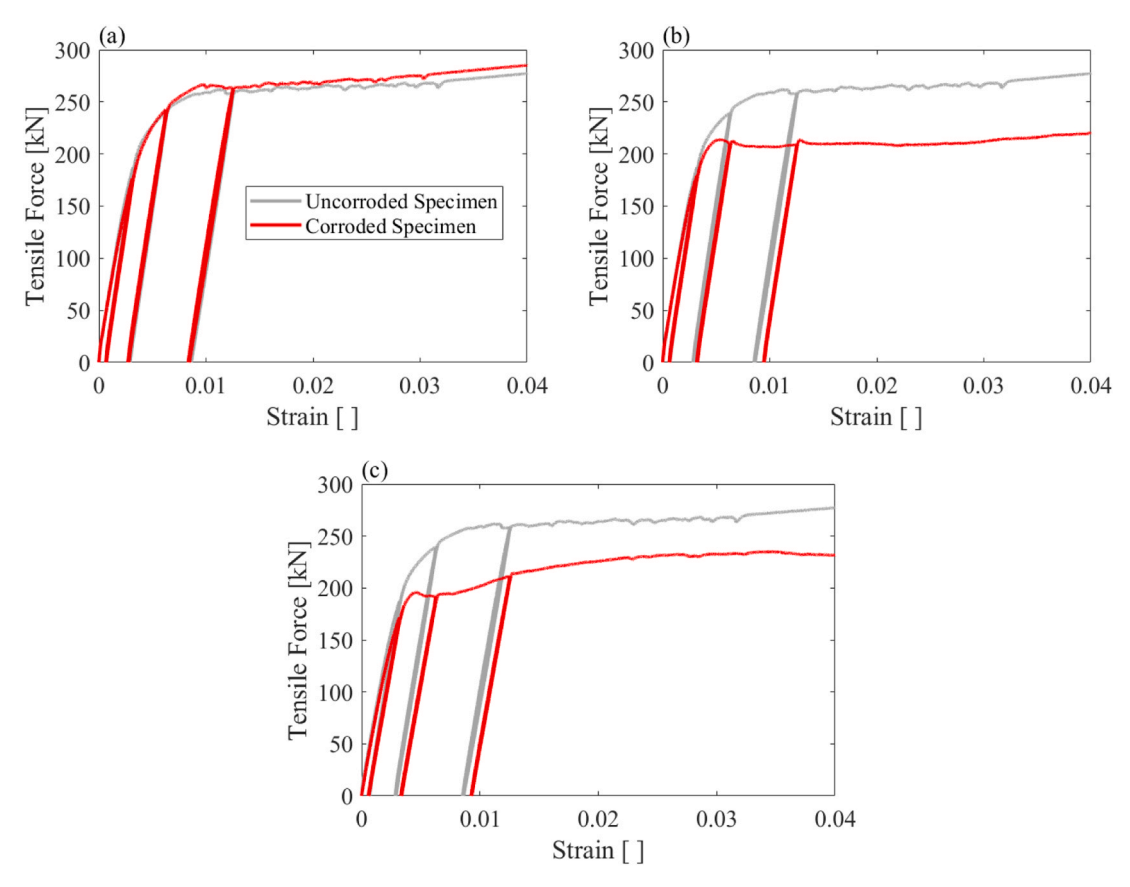


Fig. 15. Cyclic test results, SCΦ25: (a) 4.3 % corrosion, (b) 12 % corrosion, and (c) 22.1 % corrosion.

specimens was more uniform than the specimens with 20 mm diameter bars.

3.1. Discussion of the influence of corrosion on concrete cracking and crack pattern

The changes in crack patterns and the timing of the first cracking in corroded RC specimens can be attributed primarily to the deterioration of the bond between concrete and steel reinforcement, loss of cross-sectional area, and internal stresses due to corrosion products. As corrosion progresses, it introduces expansive rust products that apply pressure on the surrounding concrete. This pressure initiates radial tensile stresses, which result in longitudinal cracking along the reinforcement, especially at higher corrosion levels.

At low corrosion levels ($\leq \sim 8$ %), the corrosion tends to enhance the bond strength initially due to the slight expansion of corrosion products, which increases confinement at the steel-concrete interface. This sometimes even leads to marginal improvements in tensile force capacity, as observed in both our monotonic and cyclic test results.

However, at higher corrosion levels (>~10–12 %), the accumulation of corrosion products leads to extensive cracking and degradation of the steel-concrete bond, resulting in longitudinal cracking and debonding, particularly evident in the DIC strain contours. These effects disrupt the tension stiffening mechanism and lead to significant reductions in tensile capacity, earlier cracking, and degradation under cyclic loading. Additionally, high corrosion levels were associated with localised pitting, which led to premature failure in some specimens.

As explained above, initially, lateral cracks dominate at low corrosion levels, indicating preserved bond integrity and efficient tension stiffening. However, at advanced corrosion levels (e.g., 12.4% and 18.3%), the specimens show a transition to dominant longitudinal cracks, showing significant bond deterioration or complete debonding

between the steel and concrete. Moreover, corrosion causes localised pitting, which weakens the rebar more significantly than uniform corrosion. This leads to stress concentrations, reducing the effective tensile capacity of the steel. Consequently, the RC specimens crack at lower tensile strains and forces, as seen in the early failure of the 8.4 % corroded specimen due to a large local pit. In addition, weakened bond strength shifts more of the tensile force to the reinforcement early, thereby triggering earlier cracking compared to uncorroded specimens. The build-up of corrosion products within the concrete also introduces internal microcracks and tensile stresses even before any external load is applied. This pre-existing damage reduces the strain threshold needed for cracking under tensile loads, thereby advancing the onset of the first crack. Further research is required using Computing Tomography Scan (CT scan) to be able to quantify the influence of internal corrosion damage on tension stiffening behaviour.

Despite the significant influence on crack pattern and time of first crack, crack spacing remains relatively unaffected by corrosion in this study. This is because the spacing of cracks is primarily influenced by the bond strength and reinforcement ratio, which govern the distribution of tensile stresses in the concrete between cracks. At initial cracking stages, even corroded specimens exhibit some residual bond, enough to control the distribution of tensile strains and allow the formation of multiple cracks at roughly regular intervals. Although corrosion reduces bond strength, this effect becomes critical only at higher strain levels, when longitudinal cracks dominate. For the initial crack spacing, especially in specimens with corrosion levels below ~10 %, the degradation is not yet severe enough to disrupt the uniform stress transfer between reinforcement and concrete. Hence, the measured crack spacing remains close to that of uncorroded specimens, even as crack width increases. Crack spacing is strongly influenced by the bar diameter-to-concrete cover ratio, reinforcement arrangement, and concrete tensile strength, all of which remain constant across specimens. Since the test specimens maintained consistent geometry and material properties, and because the bond degradation was not yet fully destructive during early loading, crack spacing did not significantly deviate even with corrosion.

4. Evaluation of existing crack spacing and width models

In this section, the tension stiffening crack spacing and width predictions based on fib Model Code 2010 ([62,63]) and fib Model Code 2020 [64] are evaluated using the experimental data presented in 3. The calculation of crack width in RC structures follows the guidelines provided by these models, considering factors such as the tensile strength of concrete, reinforcement properties, bond stress, etc.

The concrete properties used in the calculations include the mean tensile strength, f_{ctm} , and the mean compressive strength, f_{ctm} . The Young's modulus of concrete, E_{ctm} is calculated using an empirical formula based on the compressive strength:

$$E_{cm} = 21500 \left(\frac{f_{cm}}{10}\right)^{\frac{1}{3}} \tag{1}$$

The bond stress, τ_b , is a critical factor that influences crack formation. According to fib Model Code, it can be estimated as:

$$\tau_{\rm b} = 1.8 f_{\rm ctm} \tag{2}$$

In cases where corrosion occurs, the bond strength between the reinforcement and concrete decreases. Corrosion is quantified by the corrosion penetration depth, x_c , measured in microns, μ m. Based on fib Model Code 2020, the corrosion factor, η_{cor} , is 1 for $x_c < 50~\mu$ m, for insignificant corrosion scenarios, and reduces to 0.5 for $x_c > 200~\mu$ m, for severe corrosion cases. The effective bond stress, accounting for corrosion, is:

$$\tau_{b,cor} = \eta_{cor} \tau_b \tag{3}$$

The maximum crack spacing, s_{max} , in fib Model Code 2010 is determined using the following equation:

$$s_{\text{max},2010} = 2\left(k_{\text{c},2010}c + \frac{f_{\text{ctm}\phi}}{\rho_{\text{eff}}\tau_{\text{b}}}\right) \tag{4}$$

where $k_{c,\ 2010}=1$ is concrete cover correction factor; c is the concrete cover and ρ_{eff} is the effective reinforcement ratio. In contrast, fib Model Code 2020 refines the crack spacing formula by introducing additional coefficients:

$$s_{\text{max},2020} \quad = \quad \beta_w \Bigg(k_{\text{c},2020} c \quad + \quad k_{\text{\theta},p} k_{\text{fl}} k_{\text{b}} \frac{f_{\text{ctm}\varphi}}{\rho_{\text{eff}} \tau_{\text{b}}} \Bigg) \tag{5}$$

where $k_{c,2020}=1.5$; $k_{\theta p}=0.25$ is reinforcement factor; $k_{\it fl}=1$ is load influence factor; $k_{\it b}=0.9$ is bond efficiency factor; $\beta_{\it w}$ is 1.7 for stabilized cracking stage, and is 2 for crack formation stage. For both models, the crack width is given by:

$$w = s_{\text{max}} \Delta \varepsilon \tag{6}$$

 $\Delta \varepsilon$ is the strain difference between steel and concrete.

Table 5 summarises the measured and predicted crack spacing and width values for different bar sizes and corrosion levels. The stress and

strain, at which the first crack is generated, is taken from the Monotonic test results, shown in Figs. 10 and 14. As seen, when there is no corrosion, i.e., 0 %, the predicted crack width values are close to the predicted ones. However, as for corroded samples, the models under predict the crack width values. A mentioned above, the corrosion effects is considered in the models through corrosion factor that reduces the bond stress. For all corrosion levels studied in this work, the corrosion penetration is larger than 200 μm . Based on the models, a corrosion factor of 0.5 should be used. It appears that this corrosion factor has been determined for lower corrosion factors. Hence, further investigation on corrosion factor is required to accurately determine this factor for a wide range of corrosion levels. For bar diameter of 20 mm, fib Models predicted values are close to the measured ones. However, for bar diameter of 25 mm, the predicted spacing values are far larger than the measured ones.

5. Conclusion

This study investigates the nonlinear tension stiffening behaviour of reinforced concrete (RC) members subjected to varying levels of reinforcement corrosion under monotonic and cyclic loading. Through an extensive experimental programme involving uniaxial tensile tests on 28 RC specimens, several critical observations were made.

Corrosion significantly reduces the tension stiffening effect in RC members, particularly at higher corrosion levels (15 % and 20 %). At these levels, the concrete's ability to transfer tensile stresses between adjacent cracks is severely compromised. Crack development patterns highlight that at low corrosion levels (0 %-10 %), lateral cracks dominate, maintaining effective tension stiffening. However, as corrosion progresses, longitudinal cracks emerge due to bond deterioration, leading to the loss of tension stiffening as the bond between concrete and steel reinforcement fails.

Larger steel bar diameters exacerbate the degradation of tension stiffening. Specimens reinforced with $\Phi 25$ bars exhibited earlier onset of longitudinal cracks and more pronounced reductions in tensile capacity compared to those with $\Phi 20$ bars. Furthermore, under cyclic loading, specimens with low corrosion levels initially demonstrated an increase in tensile capacity due to enhanced bond strength. At advanced corrosion levels, however, cyclic loading accelerated failure due to the combined effects of bond degradation and reduced steel capacity.

The findings emphasise the importance of mitigating corrosion in RC structures, by proper durability considerations in the design of new structures. Furthermore, it is important to consider the effects of bond behaviour and tension stiffening in the assessment of existing substandard and corroded structures. Moreover, this research fills critical gaps in understanding the effects of high corrosion levels and cyclic loading on tension stiffening behaviour. Future studies should explore the integration of advanced materials or rehabilitation techniques to mitigate the adverse effects of corrosion, ensuring the longevity and safety of RC structures. Also, further investigation is required to develop more reliable models for prediction of crack spacing and width values of corroded structural elements.

Table 5Summary of measured and predicted spacing and crack width.

·									
Bar Diameter (mm)	Corrosion Level (%)	Load (kN)	Strain	Measured Spacing (mm)	Predicted Spacing (mm)		Measured Width (mm)) Predicted Width (mm)	
					2010	2020		2010	2020
20	0	26.5	0.00024	250	257	237	0.060	0.052	0.048
	8.4	19.1	0.00018				0.045	0.022	0.021
	12.4	17.1	0.00017				0.044	0.014	0.013
	18.3	14.1	0.00015				0.037	0.002	0.002
25	2.3	30.6	0.00025	170	216	204	0.043	0.035	0.033
	9.1	19.6	0.00018				0.031	0.010	0.010

CRediT authorship contribution statement

Ahmadi Ehsan: Writing – review & editing, Writing – original draft, Methodology, Investigation, Formal analysis, Data curation. Kashani Mohammad M: Writing – review & editing, Supervision, Methodology, Conceptualization. Aminulai Hammed: Investigation, Conceptualization.

Ethical approval (if applicable)

Ethical approval was not needed.

Funding

This research was supported by no grant/funding.

Declaration of originality

This manuscript has not been published and is not under consideration elsewhere.

Declaration of Competing Interest

The authors declare that they have no known competing financial interests or personal relationships that could have appeared to influence the work reported in this paper.

Data availability

Data will be made available on request.

References

- [1] Sagüés AA. Modeling the effects of corrosion on the lifetime of extended reinforced concrete structures. Corrosion 2003;59. https://doi.org/10.5006/1.3287706.
- [2] Melchers RE. The effect of corrosion on the structural reliability of steel offshore structures. Corros Sci 2005;47. https://doi.org/10.1016/j.corsci.2005.04.004.
- [3] Luo X, Cheng J, Xiang P, Long H. Seismic behavior of corroded reinforced concrete column joints under low-cyclic repeated loading. Arch Civ Mech Eng 2020;20. https://doi.org/10.1007/s43452-020-00043-z.
- [4] Penttala V. Causes and mechanisms of deterioration in reinforced concrete. Fail, Distress Repair Concr Struct 2009. https://doi.org/10.1533/9781845697037.1.3.
- [5] Apostolopoulos CA. Mechanical behavior of corroded reinforcing steel bars \$500s tempcore under low cycle fatigue. Constr Build Mater 2007;21. https://doi.org/10.1016/j.conbuildmat.2006.07.008.
- [6] François R, Khan I, Dang VH. Impact of corrosion on mechanical properties of steel embedded in 27-year-old corroded reinforced concrete beams. Mater Struct/Mater Et Constr 2013;46. https://doi.org/10.1617/s11527-012-9941-z.
- [7] Imperatore S, Rinaldi Z, Drago C. Degradation relationships for the mechanical properties of corroded steel rebars. Constr Build Mater 2017;148. https://doi.org/ 10.1016/j.conbuildmat.2017.04.209.
- [8] Kashani MM, Crewe AJ, Alexander NA. Nonlinear stress-strain behaviour of corrosion-damaged reinforcing bars including inelastic buckling. Eng Struct 2013; 48. https://doi.org/10.1016/j.engstruct.2012.09.034.
- [9] Alonso C, Andrade C, Rodriguez J, Diez JM. Factors controlling cracking of concrete affected by reinforcement corrosion. Mater Struct/Mater Et Constr 1996; 31. https://doi.org/10.1007/bf02480466.
- [10] Cabrera JG. Deterioration of concrete due to reinforcement steel corrosion. Cem Concr Compos 1996;18. https://doi.org/10.1016/0958-9465(95)00043-7.
- [11] Angst U, Elsener B, Jamali A, Adey B. Concrete cover cracking owing to reinforcement corrosion - Theoretical considerations and practical experience. Mater Corros 2012;63. https://doi.org/10.1002/maco.201206669.
- [12] Bossio A, Lignola GP, Fabbrocino F, Monetta T, Prota A, Bellucci F, et al. Nondestructive assessment of corrosion of reinforcing bars through surface concrete cracks. Struct Concr 2017;18. https://doi.org/10.1002/suco.201600034.
- [13] Vidal T, Castel A, François R. Analyzing crack width to predict corrosion in reinforced concrete. Cem Concr Res 2004;34. https://doi.org/10.1016/S0008-8846(03)00246-1.
- [14] Vu NS, Yu B, Li B. Prediction of strength and drift capacity of corroded reinforced concrete columns. Constr Build Mater 2016;115. https://doi.org/10.1016/j. conbuildmat.2016.04.048.
- [15] Clark YG, Chan LA. AHC. Residual capacity of corroded reinforcing bars. Mag Concr Res 2005;57. https://doi.org/10.1680/macr.2005.57.3.135.
- [16] Vu NS, Li B. Seismic performance assessment of corroded reinforced concrete short columns. J Struct Eng 2018;144. https://doi.org/10.1061/(asce)st.1943-541x.0001994.

- [17] Goksu C, Ilki A. Seismic behavior of reinforced concrete columns with corroded deformed reinforcing bars. Acids Struct J 2016;113. https://doi.org/10.14359/ 51689030
- [18] Prakhya GKV, Morley CT. Tension-stiffening and moment-curvature relations of reinforced concrete elements. Acids Struct J 1990;87. https://doi.org/10.14359/ 2680.
- [19] Gopalaratnam V.S., Shah S.P. Softening response of plain concrete in direct tension. Journal of the American Concrete Institute 1985;82. https://doi. org/10.1016/0148-9062(86)91965-0.
- [20] Bischoff PH. Tension stiffening and cracking of steel fiber-reinforced concrete. J Mater Civ Eng 2003;15. https://doi.org/10.1061/(asce)0899-1561(2003)15:2 (174).
- [21] Bischoff PH. Tension stiffening and cracking of steel fiber-reinforced concrete. J Mater Civ Eng 2003;15:174–82. https://doi.org/10.1061/(ASCE)0899-1561 (2003)15:2(174)
- [22] Bischoff PH. Effects of shrinkage on tension stiffening and cracking in reinforced concrete. Can J Civ Eng 2001;28:363–74. https://doi.org/10.1139/100-117.
- [23] Syll AS, Shimokobe H, Kanakubo T. Effect of local bond behavior degradation on tension stiffness in reinforced concrete with pre-existing longitudinal cracks. Case Stud Constr Mater 2024;20:e03017. https://doi.org/10.1016/j.cscm.2024.e03017.
- [24] Lárusson L, Fischer G, Jönsson J. Mech Interact Concr Struct Reinf Tens Stiffening Process 2012:247–54. https://doi.org/10.1007/978-94-007-2436-5_30.
- [25] Lee Seong-Cheol, Cho Jae-Yeol, Vecchio F. Tension-stiffening model for steel fiber-reinforced concrete containing conventional reinforcement. Acids Struct J 2013; 110. https://doi.org/10.14359/51685749.
- [26] Reinhardt HW, Cornelissen HAW, Hordijk DA. Tensile tests and failure analysis of concrete. J Struct Eng 1986;112:2462–77. https://doi.org/10.1061/(ASCE)0733-9445(1986)112:11(2462).
- [27] Grisaro HY. Modeling one-dimensional tension stiffening of plain and fiber reinforced concrete with discrete cracks. 111929 Int J Solids Struct 2022:254–5. https://doi.org/10.1016/j.ijsolstr.2022.111929.
- [28] Martins MP, Rangel CS, Amario M, Lima JMF, Lima PRL, Toledo Filho RD. Modelling of tension stiffening effect in reinforced recycled concrete. Rev IBRACON De Estrut e Mater 2020;13. https://doi.org/10.1590/s1983-41952020000600005.
- [29] Fang C, Lundgren K, Chen L, Zhu C. Corrosion influence on bond in reinforced concrete. Cem Concr Res 2004;34. https://doi.org/10.1016/j. cemconres.2004.04.006.
- [30] Law DW, Molyneaux TCK. Impact of corrosion on bond in uncracked concrete with confined and unconfined rebar. Constr Build Mater 2017;155. https://doi.org/ 10.1016/j.conbuildmat.2017.08.112.
- [31] Lundgren K. Effect of corrosion on the bond between steel and concrete: an overview. Mag Concr Res 2007;59. https://doi.org/10.1680/macr.2007.59.6.447
- [32] Prieto M, Tanner P, Andrade C. Bond response in structural concrete with corroded steel bars. experimental results. RILEM Book 2011;5. https://doi.org/10.1007/ 978-94-007-0677-4 16.
- [33] Tondolo F. Bond behaviour with reinforcement corrosion. Constr Build Mater 2015;93. https://doi.org/10.1016/j.conbuildmat.2015.05.067.
- [34] Yalciner H, Eren O, Sensoy S. An experimental study on the bond strength between reinforcement bars and concrete as a function of concrete cover, strength and corrosion level. Cem Concr Res 2012;42. https://doi.org/10.1016/j. cemconres.2012.01.003.
- [35] Lin H, Zhao Y, Feng P, Ye H, Ozbolt J, Jiang C, et al. State-of-the-art review on the bond properties of corroded reinforcing steel bar. Constr Build Mater 2019;213. https://doi.org/10.1016/j.conbuildmat.2019.04.077.
- [36] Kashani MM, Maddocks J, Dizaj EA. Residual capacity of corroded reinforced concrete bridge components: state-of-the-Art Review. J Bridge Eng 2019;24. https://doi.org/10.1061/(asce)be.1943-5592.0001429.
- [37] El-Sayed AK, Hussain RR, Shuraim AB. Influence of stirrup corrosion on shear strength of reinforced concrete slender beams. Acids Struct J 2016;113. https://doi.org/10.14359/51689147.
- [38] Yalciner H, Kumbasaroglu A, El-Sayed AK, Balkis AP, Dogru E, Turan AI, et al. Flexural strength of corroded reinforced concrete beams. Acids Struct J 2020;117. https://doi.org/10.14359/51720195.
- [39] Dang VH, François R. Influence of long-term corrosion in chloride environment on mechanical behaviour of RC beam. Eng Struct 2013;48. https://doi.org/10.1016/j. engstruct.2012.09.021.
- [40] Chen HP, Nepal J. Modeling residual flexural strength of corroded reinforced concrete beams. Acids Struct J 2018;115. https://doi.org/10.14359/51702232
- [41] Jnaid F, Aboutaha RS. Residual flexural strength of corroded reinforced concrete beams. Eng Struct 2016;119. https://doi.org/10.1016/j.engstruct.2016.04.018.
- [42] Aminulai HO, Robinson AF, Ferguson NS, Kashani MM. Nonlinear behaviour of corrosion damaged low-strength short reinforced concrete columns under compressive axial cyclic loading. Eng Struct 2023;289. https://doi.org/10.1016/j. engstruct.2023.116245.
- [43] Meda A, Mostosi S, Rinaldi Z, Riva P. Experimental evaluation of the corrosion influence on the cyclic behaviour of RC columns. Eng Struct 2014;76. https://doi. org/10.1016/j.engstruct.2014.06.043.
- [44] Yang SY, Song XB, Jia HX, Chen X, Liu X. La. Experimental research on hysteretic behaviors of corroded reinforced concrete columns with different maximum amounts of corrosion of rebar. Constr Build Mater 2016;121. https://doi.org/ 10.1016/j.conbuildmat.2016.06.002.
- [45] Meda A, Mostosi S, Rinaldi Z, Riva P. Corroded RC columns repair and strengthening with high performance fiber reinforced concrete jacket. Mater Struct/Mater Et Constr 2016;49. https://doi.org/10.1617/s11527-015-0627-1.

- [46] Rajput AS, Sharma UK. Seismic behavior of under confined square reinforced concrete columns. Structures 2018;13. https://doi.org/10.1016/j. istruc.2017.10.005.
- [47] Dai KY, Lu DG, Yu XH. Experimental investigation on the seismic performance of corroded reinforced concrete columns designed with low and high axial load ratios. J Build Eng 2021;44. https://doi.org/10.1016/j.jobe.2021.102615.
- [48] Matthews B, Palermo A, Scott A. Overview of the cyclic response of reinforced concrete members subjected to artificial chloride-induced corrosion. Struct Concr 2023;24. https://doi.org/10.1002/suco.202200365.
- [49] Choi MH, Lee CH. Seismic behavior of existing reinforced concrete columns with non-seismic details under low axial loads. Materials 2022;15. https://doi.org/ 10.3390/ma15031239.
- [50] Stella A, Di Carlo F, Berto L, Talledo DA, Meda A, Rinaldi Z, et al. Testing and modelling the flexural response of reinforced concrete beams affected by pitting corrosion. Eng Struct 2024;320:118456. https://doi.org/10.1016/j. epstruct 2024 118456
- [51] Imperatore S, Rinaldi Z, Spagnuolo S. Influence of corrosion on the experimental behaviour of R.C. ties. Eng Struct 2019;198. https://doi.org/10.1016/j. engstruct.2019.109458.
- [52] The British Standards, Steel for the reinforcement of concrete Weldable reinforcing steel — General, in BS EN 10080:2005. London, UK: 2005.
- [53] The British Standards, Steel for the reinforcement of concrete Weldable reinforcing steel — Bar, coil and decoiled product — Specification, in BS 4449-2005+A3-2016. London, UK: 2016.
- [54] The British Standards, Part 5: Testing hardened concrete Flexural strength of test specimen, in BS EN 12390-5:2019. London, UK: 2019.
- [55] The British Standards, Metallic materials Tensile testing, Part 1: Method of test at room temperature, in BS EN ISO 6892–1:2019. London, UK: 2020.

- [56] Yuan Y, Ji Y, Shah SP. Comparison of two accelerated corrosion techniques for concrete structures. Acids Struct J 2007;104. https://doi.org/10.14359/18624.
- [57] Shen D, Li M, Liu C, Kang J, Li C, Yang J. Seismic performance of corroded reinforced concrete beam-column joints repaired with BFRP sheets. Constr Build Mater 2021;307. https://doi.org/10.1016/j.conbuildmat.2021.124731.
- [58] Hou L, Zhou B, Guo S, Aslani F, Chen D. Corrosion behavior and flexural performance of reinforced concrete/ultrahigh toughness cementitious composite (RC/UHTCC) beams under sustained loading and shrinkage cracking. Constr Build Mater 2019;198. https://doi.org/10.1016/j.conbuildmat.2018.11.237.
- [59] Mak MWT, Desnerck P, Lees JM. Corrosion-induced cracking and bond strength in reinforced concrete. Constr Build Mater 2019;208. https://doi.org/10.1016/j. conbuildmat.2019.02.151.
- [60] ASTM, G1-03, Standard practice for preparing, cleaning, and evaluating corrosion test specimens. ASTM International: 2011.
- [61] European Standard. EN 1992-1-1 Eurocode 2: Design of Concrete Structures Part 1-1: General Rules and Rules for Buildings. The European Union Standard 2011;1.
- [62] Imperatore S, Rinaldi Z, Spagnuolo S. Influence of corrosion on the experimental behaviour of R.C. ties. Eng Struct 2019;198:109458. https://doi.org/10.1016/j. engstruct.2019.109458.
- [63] Balázs GL, Bisch P, Borosnyói A, Burdet O, Burns C, Ceroni F, et al. Design for SLS according to fib Model Code 2010. Struct Concr 2013;14:99–123. https://doi.org/ 10.1002/suco.201200060.
- [64] Terjesen O, Pinto G, Kanstad T, Tan R. Performance study of crack width calculation methods according to Eurocodes, fib model codes and the modified tension chord model. Struct Concr 2024;25:2375–99. https://doi.org/10.1002/ suco.202300367.